Mon. Not. R. Astron. Soc. **000**, 000–000 (0000) Printed 11 August 2025 (MN LATEX style file v1.3)

A Fourier Technique for the Determination of Rotation Measures

N.E.B. Killeen[1], C.J. Fluke[2], Jun-Hui Zhao[3], & R.D.Ekers[1].

[1] *Australia Telescope National Facility, CSIRO, P.O. Box 76, Epping, N.S.W., 1710, Australia*
[2] *School of Physics, The University of Melbourne, Parkville, Vic, 3052, Australia*
[3] *Harvard-Smithsonian Center for Astrophysics, Boston, USA.*

27 Aug 2000

ABSTRACT

The traditional approach to measuring the rotation measure (RM) from radio polarimetric data consists of fitting linear polarization position angles obtained at different wavelengths to a λ^2 law. Depending exactly upon the observational instrumental parameters (e.g. bandwidth, frequency etc.), this approach suffers variously from the following malaises; $n * \pi$ ambiguity, bandwidth depolarization, bad characteristics at low signal-to-noise ratios, and it is only valid for an RM distribution which is singly valued.

In this paper, we describe a new Fourier-based technique for extracting RMs from radio polarimetric data that addresses the above problems. In particular, it deals with low signal-to-noise observations correctly, allows the recovery of a spatially unresolved RM distribution (i.e. one or more RM components) and does not suffer from an ambiguity problem. Because this technique uses observations with many closely spaced channels, it also mitigates bandwidth depolarization (but cannot escape it entirely).

Key words: Rotation Measure, Fourier Techniques, polarization, magnetic fields, radio astronomy

1 INTRODUCTION

Polarimetric analysis of the electromagnetic radiation emitted by astrophysical objects is a powerful tool which enables assessment of physical quantities such as the emission mechanism, the magnetic field, the thermal number density, and the physical geometry of the source.

In radio astronomy, it is common to try to determine a quantity called the rotation measure (RM); it is derived from the position angle of the plane of linear polarization of the signal measured at different frequencies. It describes the amount by which that plane will be rotated by Faraday rotation (Faraday 1844) owing to any magneto-ionic material between the emission and detection of the emission. The RM is often used to determine the intrinsic position angle of the projected magnetic field of the emitting object. Of course, it can also be used to probe the intervening magneto-ionic medium. However, it should be noted that the analysis of such data becomes arcane when the Faraday rotating medium is mixed in with the emitting medium.

Traditionally, the RM is extracted from broadband continuum measurements made at different frequencies by fitting a λ^2 law to the linear polarization position angles. However, this technique is compromised by several effects. First, if the plane of polarization rotates more than a turn between successive frequencies, the measurement of its position angle is ambiguous, causing the deduced RM to be in error. Second, if the RM is sufficiently large, the plane of polarization rotates substantially across the bandwidth causing degradation of the averaged signal (bandwidth depolarization). Third, any RM distribution other than one with a single value will invalidate the use of a λ^2 law. Associated with non-singly valued and unresolved RM distributions is beam depolarization; this occurs because the position angle of the polarization changes across the beam. Fourth, it incorrectly handles the noise characteristics of the signal when the signal-to-noise ratio is poor.

In this paper, we discuss a new Fourier-based technique to extract RMs from data that would otherwise be compromised by some combination of the problems listed above. It uses observations at regular, closely spaced frequencies (channels). It handles low signal-to-noise observations optimally and does not suffer from an ambiguity problem. Provided the signal *per channel* has not been completely beam depolarized by large spatial RM gradients, or completely bandwidth depolarized by large RM values, it can recover

an unresolved RM distribution. In addition, depending upon the flexibility of a particular instrument to provide combinations of channel width and number of channels (with full polarization capability), very large RMs can be accessed (up to 10^9 rad m^{-2} with the Australia Telescope Compact Array).

The Fourier technique has wide astrophysical applicability; it will be important for any object with polarized emission that has traversed regions of high electron density threaded by a strong magnetic field. Such material surrounds the nuclei of galaxies (e.g. Sgr A) and inhabits the broad-line regions of AGNs. Radio galaxies are also found with large RMs in rich clusters of galaxies owing to the large path lengths.

After we began this work, we became aware of the work of de Bruyn (1996, see Section 3.2 for details) for use with WSRT data. de Bruyn's technique is essentially equivalent to ours, although approached from a slightly different perspective.

In this paper we will refer variously to Faraday screens, distributions and components. By screen we are really referring to the physical material. By component we are really referring to a delta function within a more general mathematical distribution. We will not be too rigorous about using these terms totally consistently!

We will also assume throughout this paper that the only propagational effect that the RM screens have is to rotate the plane of linear polarization. That is, we will ignore all scattering mechanisms.

In Section 2, we describe the problems affecting the traditional approach to RM extraction. In Section 3 we describe the Fourier approach. In Section 4 we offer numerical simulations exploring this new method. We summarise our findings in Section 5. Appendix A gives a table relevant to the Australia Telescope Compact Array, indicating the range of RMs that are accessible with this instrument and the Fourier technique.

2 THE TRADITIONAL APPROACH

2.1 Definitions

We will discuss the state of the electromagnetic wave in terms of the Stokes parameters (Stokes 1852). These are copiously described in text books (e.g. Kraus, 1966). The total intensity is given the symbol I, the two components of linear polarization are symbolized by Q and U, and V represents the circularly polarized component. It is convenient to refer to the complex linear polarization introduced by Conway & Kronberg (1969), where

$$P = Q + iU = pe^{2i\psi}, \tag{1}$$

$p = \sqrt{(Q^2 + U^2)}$ is the total linearly polarized intensity and $\psi = \frac{1}{2}\tan^{-1}(U/Q)$ is the position angle of the linearly polarized radiation.

Faraday rotation is also treated extensively in the literature (xxx 19xx) and so we make no basic derivations here. The RM is defined by

$$\mathrm{RM} = 8.1 \times 10^5 \int_0^L B_\parallel N_e \mathrm{d}l \ \text{ rad m}^{-2}, \tag{2}$$

where $B_\parallel$ is the line-of-sight component of the magnetic field in Gauss, N_e is the electron density in cm^{-3} and dl is the path length in pc. The position angle, in radians, of a linearly polarized wave that has traversed a Faraday screen is given by

$$\psi = \psi_{\mathrm{in}} + \mathrm{RM}\lambda^2, \tag{3}$$

where ψ_{in} is the intrinsic position angle of the radiation, and λ is the wavelength in metres.

Traditionally, the RM is obtained by computing the position angle at a number of different wavelengths. Suppose N_λ measurements are made ($\lambda = \lambda_1 \ldots \lambda_{N_\lambda}$) of the position angle ($\psi = \psi_1 \ldots \psi_{N_\lambda}$), then the RM may be recovered with a least–squares fit to a straight line in the ψ–λ^2 plane.

2.2 Ambiguity

It is readily apparent that an ambiguity can occur in the RM recovered with this least-squares fitting when the RM is sufficiently large that ψ changes by more than π rad between adjacent wavelengths. This is commonly referred to as the '$n * \pi$ ambiguity'. With just two wavelengths, it is impossible to assess whether there are ambiguity problems or not. With three or more, a consistent solution can be found, but one must always make the assumption that the closest spaced wavelengths are themselves not subject to ambiguity. Alternatively, if you do not assume that the closest spaced wavelengths are free of ambiguity, then usually the algorithm is designed to return the lowest-valued solution or the solution with the best fit; neither is guaranteed to be correct.

An extreme example of ambiguity is demonstrated in Fig 1, where the fit to ψ–λ^2 suggests a RM of 10 rad m^{-2}, when the Faraday screen in reality has RM = 180 rad m^{-2}.

2.3 Bandwidth depolarization

Assuming that p is independent of frequency, the integrated complex polarization over bandwidth is

$$P_{\mathrm{I},\nu} = p \int_{\nu_1}^{\nu_2} e^{2i\psi(\nu)} \mathrm{d}\nu. \tag{4}$$

Substituting the expression for the position angle given by eq. (3), putting $\psi_{\mathrm{in}} = 0$ without loss of generality, and assuming the fractional bandwidth $\Delta\nu/\nu \ll 1$, one can straightforwardly show the well-known formula

$$P_{\mathrm{I},\nu} = p\frac{\sin(\alpha)}{\alpha} e^{i2\mathrm{RM}\lambda_{\mathrm{c}}{}^2} \tag{5}$$

where $\alpha = 2\mathrm{RM}\lambda_{\mathrm{c}}^2\Delta\nu/\nu_{\mathrm{c}}$, λ_{c} is the wavelength equivalent to the central frequency, $\nu_{\mathrm{c}} = (\nu_1 + \nu_2)/2$.

Fig. 2 shows a plot of the amplitude as the RM is varied for a typical choice of frequency (1.4 GHz) and a range of bandwidths from 1 to 100 MHz. Clearly RM values of several thousand are only accessible with narrow bandwidths which require high sensitivity. Naturally, for higher frequencies and narrower bandwidths, the effect is smaller; however, this plot is just for illustrative purposes to show that bandwidth depolarization is not uncommon in broadband radio observations, since RM values of several hundred rad m^{-2} are common and narrowband, single-frequency continuum observations are rare.

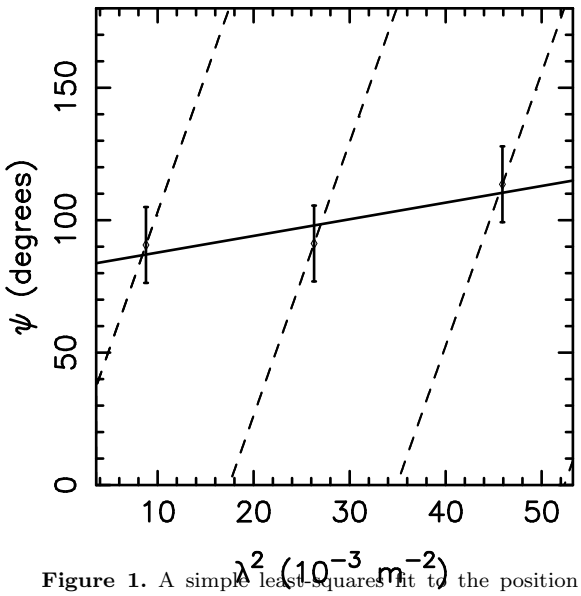

Figure 1. A simple least-squares fit to the position angle, ψ, measured at three frequencies (ν = 1.4, 1.85 and 3.2 GHz) for a Faraday screen with rotation measure RM = 180 rad m^{-2} results in an incorrect measurement of RM = 10 rad m^{-2}. The true variation of ψ with λ is shown by the dashed line. Note that ψ takes on values between 0° and 180° only. In practice, frequencies which are much more closely spaced than suggested here would be used.

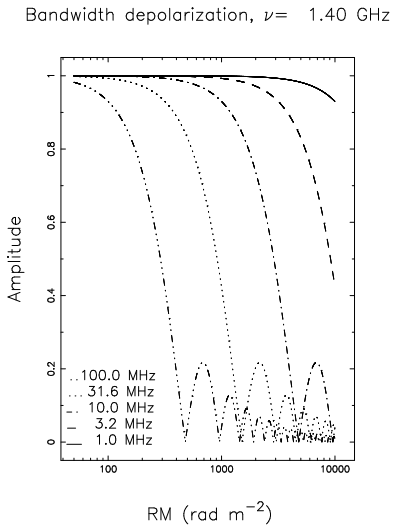

Figure 2. Bandwidth depolarization at ν_0 = 1.4 GHz and bandwidths from 1 to 100 MHz.

2.4 Noise

The traditional approach does not handle the noise characteristics of the signal optimally. Imagine that we have Q and U measurements at a number of closely spaced frequencies (e.g. regular channels). We would compute the position angle for each channel, and then, by least-squares, fit equation eq. (3) to the spectrum of position angles.

The problem here is that the position angle, $\psi(\nu)$, is computed from the noisy quantities, $Q(\nu)$ and $U(\nu)$. Referring to Fig 3, the true linear polarization of the source,

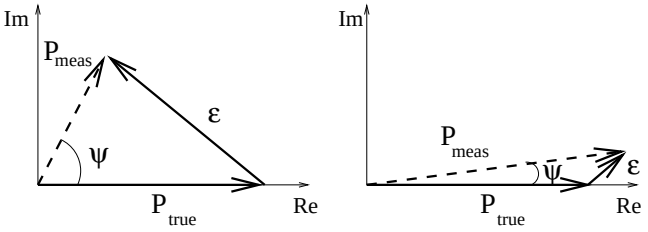

Figure 3. The measured polarization vector $\boldsymbol{P}_{\rm meas}$, and inferred position angle, ψ, depend on the true polarization vector, $\boldsymbol{P}_{\rm true}$, and the contribution from noise and calibration errors $\boldsymbol{\varepsilon}$. For convenience, $\boldsymbol{P}_{\rm true}$ has been aligned with the Real axis. (left) If the signal-to-noise ratio is small, the position angle is incorrectly measured as ψ, and so the true value is not recoverable. (right) Increasing the signal-to-noise ratio leads to a significant reduction in the inferred ψ.

$\boldsymbol{P}_{\rm true}$ is a vector in the complex plane. Noise and calibration errors add to this a vector $\boldsymbol{\varepsilon}$, so that the measured linear polarization is $\boldsymbol{P}_{\rm meas} = \boldsymbol{P}_{\rm true} + \boldsymbol{\varepsilon}$. If the signal-to-noise ratio is low, then $|\boldsymbol{P}_{\rm true}| \sim |\boldsymbol{\varepsilon}|$. In such cases, the conventional approach of computing the position angle for each channel would lead to a spectrum of noise, rather than a spectrum of meaningful position angles.

For Gaussian noise, ψ follows a symmetric distribution which becomes Gaussian at large signal-to-noise ratios. The amplitude of $\boldsymbol{P}_{\rm meas}$ is biased and follows the Rice distribution (Vinokur 1965; Wardle & Kronberg, 1974), but also becomes Gaussian for large signal-to-noise ratios. A discussion of these distributions can also be found in Thompson, Moran & Swenson (1994) and plots of both the amplitude and position angle can be seen in their figure 6.8. As the available signal-to-noise ratio increases, the symmetric spread in measured ψ about the true value will decrease.

2.5 More Complex RM Distributions

The traditional approach fails for any spatially unresolved RM distribution other than one that is singly valued. As shown in the top two panels of Fig. 4, the functional form of eq. (3) will correctly fit a single RM component (provided observations can be made at sufficiently closely spaced wavelengths to avoid ambiguity problems). However, adding one (or more) additional Faraday components (lower panel of Fig. 4) causes the linear model of eq. (3) to be invalid. In this example, the gradient is intermediate between the two input RM values, but with discontinuities in $\psi < 180°$.

One should also be aware of beam depolarization. This means that if there are RM gradients unresolved to the telescope beam, the vector sum over the beam of the complex polarization will degrade the signal strength. By how much depends upon the exact form of the gradients, but it can potentially completely depolarize the signal. Analytic solutions for simple linear RM gradients have been obtained by Leahy et al. (19xx).

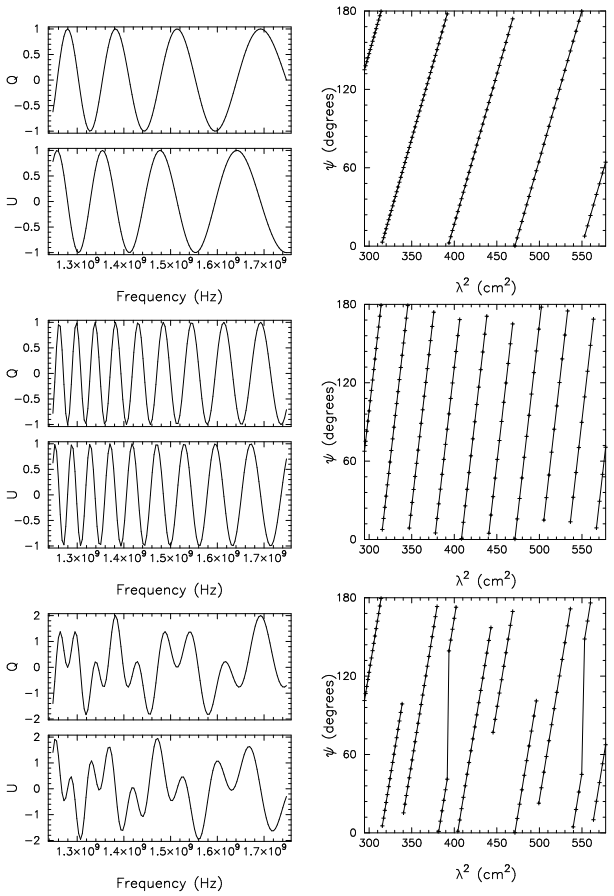

Figure 4. Position-angle variation for multiple Faraday components. The left-hand column shows Stokes Q,U data as a function of frequency; the right-hand column plots position angle, $\psi \in [0, 180]$ degrees, versus λ^2. The plots cover a bandwidth of 500 MHz in 128 (equally spaced in frequency) channels centred on 1.5 GHz. The input RM models are (top) single RM = 400 rad m^{-2}, (middle) single RM = 1000 rad m^{-2} and (bottom) multiple RM = 400 and RM = 1000 rad m^{-2}. Clearly, when multiple Faraday components are present, the linear ψ–λ^2 relation no longer holds: a least-squares fit to to a small number of (ψ,λ) data points would give an incorrect estimate of the RM.

3 THE FOURIER TECHNIQUE

3.1 Overview

Our new technique is a simple Fourier-based idea, facilitated by modern correlator capabilities. Instead of making broadband continuum observations at a few frequencies, one obtains many closely spaced continuum channels over a broad band. This is no different from a spectral-line observation. Of course such observations have been made in the past, and these decreased the ambiguity and bandwidth depolarization problems. However, the analysis was still done in the traditional way and therefore still suffer from the other problems described above.

We will show in this section that our Fourier approach to multichannel polarimetric observations is not subject to ambiguity, handles noise optimally (allowing us to detect RMs at much lower signal-to-noise ratios than with the traditional approach) and may also allow us to recover an RM distribution (i.e. one that is more complex than a single value) unresolved to the telescope beam. Because it uses multichannel observations over a broader band, it retains the benefits of reduced bandwidth depolarization. However, sufficiently large RM values which completely bandwidth depolarize a *single channel*, or unresolved RM distributions that completely beam depolarize the signal, will still render this technique ineffective.

Consider the observation of a point source with a multichannel correlator configuration over some broad bandwidth. From this we can produce a real valued spectrum (in the image domain) for each of the Stokes parameters. The next step is to form the complex spectrum $P(\nu) = Q(\nu) + iU(\nu) = p(\nu)e^{2i\psi(\nu)}$. If the RM is singly valued and non-zero, ψ changes with frequency according to eq. (3) and we have a complex (quasi) exponential.

One can imagine a least-squares fit (of the appropriate λ^2 function) to the $P = Q + iU$ spectrum (essentially a simultaneous fit of Q and U; this is *not* the same as fitting the position angle to λ^2) which would recover the RM and not be subject to broadband bandwidth depolarization. Alternatively, in the limit that the fractional total bandwidth is small (i.e. the λ^2 stretching over the bandwidth can be ignored), $P(\nu)$ is an exponential, and the Fourier transform of $P(\nu)$ is a delta function in time space. The location of that delta function is directly proportional to the RM. If RM = 0, P is independent of frequency, and its Fourier transform is a delta function at $t = 0$.

The Fourier (and fitting of $P(\nu)$) technique has a substantial benefit over the conventional approach with regard to signal-to-noise ratio considerations (see Section 2.4). This is because it does not compute a secondary quantity (the position angle) from the noisy Q and U values. The Q and U spectra, subject to well-behaved Gaussian noise, are effectively used simultaneously. This means substantially weaker signals can be recovered than in the traditional approach.

So far we have noted that the Fourier technique is equivalent to the approach of fitting $P(\nu)$ when the fractional bandwidth is small. However, the Fourier technique is more convenient for complex RM distributions, because it will give that distribution straight away in the transform; there is no need to decide how many RM components to fit and what the starting values are.

Consider the case where there are $N_{\rm F}$ spatially discrete Faraday screens completely filling the telescope's spatial beam (this is a very general distribution). For simplicity, let us say that the complex polarization state of the radiation impinging upon those screens is the same, and given by $P(\nu)$. The integrated response, $P_{\rm I}(\nu)$, is a vector sum over the spatial beam of the radiation for all lines of sight within the beam. Thus,

$$P_{\rm I}(\nu) = p(\nu) \sum_{k}^{N_{\rm F}} e^{i2\pi {\rm RM}_k \lambda^2} \qquad (6)$$

where we have ignored beam-response weighting factors. Rather than writing the RM effect as a phase term, one could also think of P in terms of its real (Q) and imaginary (U) components which are summed over the beam separately. The spectrum, $P_{\rm I}(\nu)$, thus contains spectral Fourier components induced by the frequency dependence of the Faraday screen; it does not consist of just one Fourier component. An example of this can be seen in the lower panels of Fig. 4

which shows Q, U, and ψ for a two-component RM distribution. Taking the Fourier transform of $P(\nu)$ yields those components, which are inaccessible with the traditional technique of fitting a spectrum of position angles for a single RM. We will put this on a firmer mathematical footing in the next Section and also in the numerical simulations of Section 4. These multiple components are of course also recoverable through least-squares fitting to the $P(\nu)$ spectrum.

A practical approach might be to use the Fourier technique to find quickly the main RM components, and then put those (discrete) locations as starting locations into a computer program which fits $P(\nu)$. However, in this paper we will concentrate on the Fourier approach only, owing to its computational speed and ease of use.

Note that if the RM screens are all along the same line of sight, then the Fourier technique cannot help. The radiation that traverses the different screens simply emerges from the last one having had its position angle rotated successively by each screen; this is indistinguishable from an RM distribution which is singly valued.

The Fourier technique not only yields the differing components of the screen, but it also offers an elegant and powerful way of visualizing the signal from all the screens. For an extended source, one makes 3-D (two spatial and one frequency dimension) images of Q and U and then Fourier transforms the complex polarization $P(\nu) = Q(\nu) + iU(\nu)$ from the frequency domain to the time domain and searches the resultant 3-D (two spatial and one time dimension) image for peaks corresponding to RM screens – different screens show up at different times (or lags) in the Fourier transformed image.

3.2 de Bruyn's Work

In de Bruyn's (1996) formulation , images of the complex quantity, $P(\nu)$, are formed for a range of broadband frequencies (which were not equally spaced). One then guesses a value for the RM, and unwinds $P(\nu)$ back to some reference frequency by applying that RM. All the images are then summed. This is repeated for a range of RM values, and a plot of the sum versus the RM can be generated for each spatial pixel in the images. The location of the peak value in the sum gives the 'best fit' RM. This is really just the inverse of the Fourier transform technique – there would be secondary peaks if there were multiple RM screens. de Bruyn's formulation is equivalent to ours, although he did not implement it with the Fourier approach, nor explore issues such as optimized signal-to-noise ratios, ambiguity, and unresolved screens that we comment upon in this paper. de Bruyn did note, however, that different spatial locations may have a different RM value which optimized the sum. He also argued that his technique would be more effective with many narrowband channels, which is the style of observation we discuss in this paper.

3.3 Mathematical Basis

In this Section we will show that, for a singly valued RM distribution, the Fourier transform of $P(\nu)$ is a delta function, the location of which is proportional to the RM, provided we make the simplifying assumption that $\Delta\nu/\nu \ll 1$ (so that the λ^2 dependence can be ignored), where $\Delta\nu$ is the total bandwidth.

Consider the complex polarization spectrum of a point source, $P(\nu)$, and its complex Fourier transform

$$\begin{aligned}\mathcal{P}(t) &= \frac{1}{\Delta\nu}\int P(\nu)e^{i2\pi\nu t}\mathrm{d}\nu \\ &= \frac{1}{\Delta\nu}\int p(\nu)e^{i2\psi}e^{i2\pi\nu t}\mathrm{d}\nu. \end{aligned} \quad (7)$$

We have used eq. (1) in deriving this. Substituting $\omega = \nu - \nu_\mathrm{c}$ (where ν_c is the central frequency of the spectrum) into this equation we find

$$\mathcal{P}(t) = \frac{e^{i2\pi\nu_\mathrm{c}t}}{\Delta\nu}\int pe^{i2\psi+i2\pi\omega t}\mathrm{d}\omega. \quad (8)$$

Because we wish to make a linear approximation of the quasi-exponential, $P(\nu)$, we make a Taylor series expansion of λ^2 as a function of frequency centred on ν_c and assume that $\omega/\nu_\mathrm{c} \ll 1$:

$$\lambda^2 = \lambda_\mathrm{c}^2 + (\lambda_\mathrm{c}^2)'\omega + \frac{(\lambda_\mathrm{c}^2)''}{2}\omega^2 + O\left[\omega^3\right], \quad (9)$$

where $\lambda_\mathrm{c} = c/\nu_\mathrm{c}$ and c is the speed of light. Substituting eq. (9) (with the definition of ω) into eq. (3), then substituting eq. (3) into eq. (8), and dropping third-order terms, it is straightforward to show that

$$\begin{aligned}\mathcal{P}(t) = \quad & \frac{pe^{i2(\mathrm{RM}\lambda_\mathrm{c}^2+\psi_\mathrm{in}+\pi\nu_\mathrm{c}t)}}{\Delta\nu} \times \\ & \int e^{i2\mathrm{RM}\left[(\lambda_\mathrm{c}^2)'\omega+\frac{(\lambda_\mathrm{c}^2)''\omega^2}{2}\right]}e^{i2\pi\omega t}\mathrm{d}\omega, \end{aligned} \quad (10)$$

where we have also assumed that p and ψ_in are frequency independent. If we now define

$$\begin{aligned}\tau_\mathrm{RM} &= \frac{\mathrm{RM}(\lambda_\mathrm{c}^2)'}{\pi} \\ &= -\frac{2}{\pi}\frac{\mathrm{RM}\lambda_\mathrm{c}^2}{\nu_\mathrm{c}}, \end{aligned} \quad (11)$$

and dismiss the second-order term in the Taylor series (i.e. make a linear approximation) we have

$$\mathcal{P}(t) = \frac{pe^{i2(RM\lambda_\mathrm{c}^2+\psi_\mathrm{in}+\pi\nu_\mathrm{c}t)}}{\Delta\nu}\int e^{i2\pi\omega(\tau_\mathrm{RM}+t)}\mathrm{d}\omega. \quad (12)$$

The integral is the delta function, $\delta(\tau_\mathrm{RM}+t)$. One measures τ_RM from the location of the peak of the amplitude of $\mathcal{P}(t)$ and then computes the RM from eq. (11).

3.4 More Complex RM Distributions

So far we have considered only a singly valued RM distribution. In Section 3.1 we argued qualitatively (see eq. 6) that if there were N_F discrete, singly valued Faraday screens completely filling the telescope's beam, then the Fourier technique would recover those components (provided beam depolarization has not completely depolarized the signal). In this Section we will show that more carefully. Since such a distribution is very general, this is a powerful result.

The measured complex polarization obtained with a finite beam is

$$P_{\rm I}(\nu) = \int\int B(x,y)p(x,y,\nu)e^{2i\psi(x,y,\nu)}{\rm d}x{\rm d}y, \quad (13)$$

where we have assumed that the beam response, $B(x,y)$, is independent of frequency over the range of frequencies observed and that its integral is unity.

Imposing the above discrete Faraday screen condition and assuming that the polarization of the incident radiation for each screen is constant and given by $p_k(\nu)$, we can write the integrated complex polarization as

$$\begin{aligned} P_{\rm I}(\nu) &= \sum_k^{N_{\rm F}} p_k(\nu)e^{2i\psi_k(\nu)} \int\int_{A_k} B(x,y){\rm d}x{\rm d}y \\ &= \sum_k^{N_{\rm F}} p_k(\nu)e^{2i\psi_k(\nu)}\mathcal{A}_k, \end{aligned} \quad (14)$$

where the $\mathcal{A}_k$ are geometrical terms giving the integral over the beam response at the location of each region. This is a more general form of eq. (6). The Fourier transform of $P_{\rm I}(\nu)$ is therefore

$$\begin{aligned} \mathcal{P}_{\rm I}(t) &= \frac{1}{\Delta\nu}\int_{-\infty}^{\infty} P_{\rm I}(\nu)e^{2\pi i\nu t}{\rm d}\nu \\ &= \frac{1}{\Delta\nu}\int \sum_k^{N_{\rm F}} \mathcal{A}_k p_k(\nu)e^{2i\psi_k(\nu)}e^{2\pi i\nu t}{\rm d}\nu \\ &= \frac{1}{\Delta\nu}\sum_k^{N_{\rm F}} \mathcal{A}_k \int p_k(\nu)e^{2i\psi_k(\nu)+2\pi i\nu t}{\rm d}\nu, \end{aligned} \quad (15)$$

where we have interchanged the order of the integral and sum to reach the last expression. Each integral term inside the sum is equivalent to Fourier transforming a singly valued RM screen, the result of which is given by eq. (12). The resultant spatially summed spectrum, $\mathcal{P}_{\rm I}(t)$, is a linear combination of the $N_{\rm F}$ terms in the sum, where the coefficients are given by the product of the beam-area weighting factor, and the incident polarized intensity. Therefore, since this is a linear process, we can recover from the amplitude spectrum, $|\mathcal{P}(t)|$, each of the RM components.

In general, we cannot recover the intrinsic polarization of the radiation incident upon each screen; it is weighted by the beam integral factor, $\mathcal{A}_k$. However, the weighting is the areal value, so, although the amplitude of the polarized intensity is lost, its position angle is recoverable. In the special case of a point source at the centre of the beam, we can also recover the intrinsic polarized intensity.

Clearly, if the RM structure is not resolved by the beam, we cannot determine where the Faraday screens are – only that there are one (or more) screens within the beam, what the RM value is for each screen, and what the weighted complex polarization of the incident radiation was. Again we emphasize that we can do this only if the signal is not completely beam depolarized.

3.5 The Detectable Rotation Measure Range

Real observations present a band-limited signal (in this case, one with finite frequency bandwidth provided by filters) to digital samplers, which results in digitized samples in time. Modern correlators then produce the frequency spectrum by Fourier transforming a finite time (lag) series (or spectrum). This means that RM values which correspond to larger time lags than the maximum computed in the correlator are not detectable.

In our procedure, we take the Q and U frequency spectra provided by the correlator (or for spatially extended sources, compute images of Stokes Q and U at each frequency channel) and then Fourier transform *back* to the time-lag space. Only the signals of RM components corresponding to time lags originally generated in the correlator will be present in the new lag spectrum. There is no RM signal aliasing in this process. Aliasing can occur only if the front-end filters have high sidelobes. Modern filter designs generally have excellent sidelobe characteristics, so this is not an issue.

With an 'XF' correlator (D'Addario 1989), one would ideally gain access to the lag spectrum, and make images for Q and U for each lag from that. However, in practice, our correlators provide us with a frequency spectrum and so we have to transform back. In addition, our calibration software is heavily frequency-space oriented. But, in principle, one could consider avoiding these two extra transforms.

The detectable RM range is found as follows. Consider a correlator which provides $N_{\rm chan}$ frequency channels over a bandwidth $\Delta\nu$ centred on $\nu_{\rm c}$, so that each channel has a width $\delta\nu$. The corresponding time-lag space also has $N_{\rm chan}$ lags, over a total time $\Delta t = 1/\delta\nu$ with lag spacing $\delta t = 1/\Delta\nu$. By choosing to perform the transform with respect to the central frequency, we have time lags centred on $t = 0$, and hence we will be able to recover RM components of either sign.

The maximum detectable RM is then given by the maximum measured time lag ($t_{\rm max} = 1/2\delta\nu$):

$${\rm RM}_{\rm max} = \frac{\pi\nu_{\rm c}t_{\rm max}}{2\lambda_{\rm c}^2} = \frac{\pi\nu_{\rm c}}{4\lambda_{\rm c}^2\delta\nu}. \quad (16)$$

The RM sampling interval is found easily from δt to be

$$\Delta{\rm RM}_{\rm samp} = \frac{\pi\nu_{\rm c}}{2\lambda_{\rm c}^2\Delta\nu}. \quad (17)$$

Note that the central lag channel* contains all signals with $|{\rm RM}| < \Delta{\rm RM}_{\rm samp}$.

3.6 Ambiguity

The Fourier technique does not suffer from an ambiguity problem because the signal is band limited and fully sampled in the time-lag (RM) domain. Any RM signal large enough to cause a position-angle rotation between adjacent channels that is in turn large enough to cause an ambiguity problem would have to be greater than ${\rm RM}_{\rm max}$. Therefore it is not detected and does no damage.

Remembering the assumption that $\Delta\nu/\nu << 1$, the

* if $N_{\rm chan}$ is odd, otherwise central two channels

position-angle change between adjacent channels at frequencies ν and $\nu + \delta\nu$ is

$$\delta\psi = -\mathrm{RM}c^2 \frac{\delta\nu}{\nu^3}. \quad (18)$$

Substituting the expression for $\mathrm{RM}_{\max}$, we find $|\delta\psi| = \pi/4 < \pi$ and so there is no $n * \pi$ ambiguity over the detectable range of RMs.

3.7 Deviations from the Ideal Case

So far, we have only treated the ideal case. We have assumed that the fractional bandwidth is small (linearity), that the frequency integration limits extend to infinity, and that there is no frequency dependence of the polarized emission. We now discuss the effects of relaxing these criteria.

3.7.1 Linearity

We can estimate when the linear assumption will start to fail by comparing the size of the first and second exponential terms in eq. (10). When they are roughly equal, the assumption of linearity will be compromised. Thus, from the equality

$$(\lambda_c^2)'\omega = \frac{(\lambda_c^2)''\omega^2}{2} \quad (19)$$

we find $\Delta\nu/\nu_c = 2/3$. The presence of a substantial second-order term essentially translates into an error in the measurement of the location of the delta function in the time domain. Since the integration limits are $\omega = \pm\nu/2$ the largest value the second order term can have is

$$\Delta t_2 = \frac{3}{2\pi}\mathrm{RM}\lambda_c^2 \frac{\Delta\nu}{\nu_c^2}. \quad (20)$$

Applying eq. (11), this translates into an error for the RM of

$$\Delta\mathrm{RM}_2 = \frac{3}{4}\mathrm{RM}\frac{\Delta\nu}{\nu_c}. \quad (21)$$

If the second order error should become important, then it can be eradicated by resampling the frequency spectrum (which is band limited) in frequency-squared space. We do not bother to do this because the second-order error is generally small, and we wish to retain computational efficiency; our data are provided to us by the correlator as a regularly sampled frequency spectrum.

3.7.2 Finite Bandwidth

We can incorporate the finite bandwidth (recall we are assuming a bandlimited frequency spectrum) by an appropriate modification of eq. (12):

$$\mathcal{P}(t) = \frac{p e^{i2(\mathrm{RM}\lambda_c^2 + \psi_{\mathrm{in}} + \pi\nu_c t)}}{\Delta\nu} \int b(\omega) e^{i2\pi\omega\tau_{\mathrm{RM}}} e^{i2\pi\omega t} \mathrm{d}\omega, \quad (22)$$

where $b(\omega)$ is the bandpass function. Since we are just dealing with the calibrated spectrum of a point source here, we can consider the bandpass shape to be a real-valued rectangle or top-hat function. It is clear from this equation and the Fourier convolution theorem that $\mathcal{P}(t)$ is not a delta function, but the convolution of the delta function and a sinc function (the Fourier transform of the top-hat function). This is of course just the sinc function. The zeros of the sinc function are at integer multiples of $\pm 1/\Delta\nu$ and the full width at half maximum is $1.2/\Delta\nu$. Since $1/\Delta\nu$ is the sampling interval of the lag spectrum, any signal exactly centred on a channel does not exhibit the sinc sidelobes.

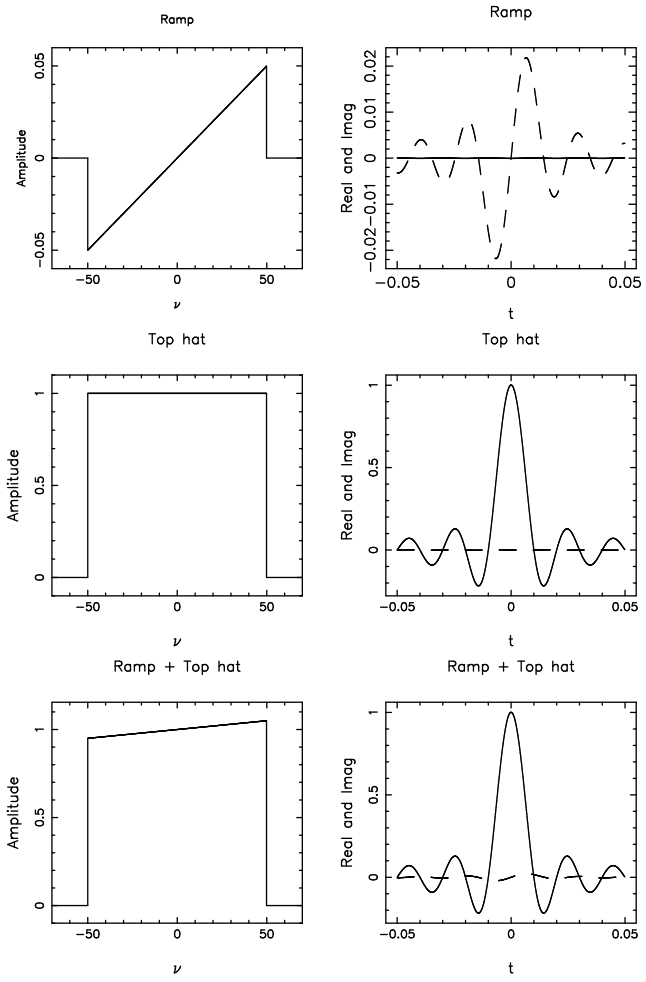

Figure 5. Truncated ramp, top-hat and sum of the ramp and top-hat functions and their Fourier transforms (real is solid, imaginary dashed).

3.7.3 Frequency Dependence

So far, we have assumed that the spectrum of linear polarization is given by

$$\begin{aligned} P(\nu) &= p(\nu)e^{2i\psi(\nu)} \\ &= p e^{2i(\psi_{\mathrm{in}} + RM\lambda^2)}. \end{aligned} \quad (23)$$

However, in reality, both the amplitude and intrinsic position angle might be frequency dependent. Let us reformulate the problem again then as

$$\mathcal{P}(t) = \frac{e^{i2(\mathrm{RM}\lambda_c^2 + \pi\nu_c t)}}{\Delta\nu} \int b(\omega)p(\omega) e^{i2\psi_{\mathrm{in}}(\nu)} e^{i2\pi\omega\tau_{\mathrm{RM}}} e^{i2\pi\omega t} \mathrm{d}\omega. \quad (24)$$

First, we consider the frequency dependence of $p(\omega)$ and

ignore the frequency dependence of $\psi_{\rm in}$. Since we are dealing with relatively narrow bandwidths, we approximate the spectrum with a linear function, into which we also incorporate the bandpass top-hat function. This is illustrated in Fig. 5. One can think of this function as the sum of the even top-hat function, and the odd truncated ramp that passes though zero. Using the linearity theorem, its Fourier transform is the sum of the real sinc function (Fourier transform of top hat) and an imaginary sinc derivative (Fourier transform of truncated ramp). These are also illustrated in Fig. 5. In the limit that the ramp is horizontal (no spectral dependence) we are left only with the sinc function as before.

At first sight this is rather unpleasant. The sinc derivative converts something symmetric and peaked at the signal, to something asymmetric and no longer centred on the signal of interest (since we search for RM peaks by looking at the amplitude it does not matter particularly that it is imaginary as well). However, its quantitative contribution to the Fourier transform depends upon the amplitude of the truncated ramp relative to the amplitude of the top hat.

For example, if the amplitude change of the ramp is 10 per cent of the height of the top hat, its contribution to the Fourier Transform is essentially negligible at 2 per cent. What spectral index would generate a 10 per cent ramp? At 1 GHz with 100 MHz bandwidth, a 10 per cent ramp gives a spectral index of unity which is already towards the limits of a typical spectral index range.

To make the fractional ramp amplitude larger, one would need to go to lower frequencies. For example, for a spectral index of 1.0, we would need a frequency of 0.2 GHz for 100 MHz bandwidth to make the fractional ramp amplitude 50 per cent. However, because the sinc derivative amplitude does not scale linearly, this still only means that the imaginary component of the Fourier transform is 10 per cent that of the real component.

We conclude that the frequency dependence of the amplitude of $P(\nu)$ is unlikely to be important.

Second, we turn to the frequency dependence of the intrinsic position angle, $\psi_{\rm in}$. Let us again assume linearity with frequency so that

$$\psi_{\rm in} = (\psi_{\rm in,0} + \beta\nu_{\rm c}) + \beta\omega. \tag{25}$$

Ignoring the frequency dependence of $p(\omega)$, eq. (24) becomes

$$\mathcal{P}(t) = \frac{p e^{i2(\mathrm{RM}\lambda_{\rm c}^2 + \pi\nu_{\rm c}t + \beta(\nu_{\rm c}+\psi_{\rm in,0}))}}{\Delta\nu} \times \int b(\omega) e^{i2\pi\omega\left(\tau_{\rm RM}+t+\frac{\beta}{\pi}\right)} \mathrm{d}\omega. \tag{26}$$

This equation shows that the effect is to offset the location of the delta function; the frequency dependence of the intrinsic position angle is effectively equivalent to modifying the value of the RM.

Of course, the real functional form of the frequency dependence might be anything; this is just a guide. This term will offset the RM peak by one channel when it is equal to the time sampling interval, i.e. when $\beta = \pi/\Delta\nu$ rad Hz^{-1}. This means that the total rotation of $\psi_{\rm in}$ across the band would be π radians.

4 NUMERICAL MODELLING OF THE FOURIER TRANSFORM TECHNIQUE

4.1 Formulation

Consider a source which is observed through $N_{\rm F}$ spatially distinct and singly valued Faraday screens which are not mixed in with the emitting material. Associated with each screen is a rotation measure RM_k.

From eq. (6), the Stokes Q and U, measured at a discrete frequency, ν_j, are given by the sum of the contributions due to each Faraday screen, with an appropriate weighting factor, $p(\nu_j)$. As a demonstration of the Fourier transform technique, we restrict our study to the idealised case where all the $p(\nu_j) = 1$, and neglect any additional effects due to the beam response (see section Section 3.4). Thus we can write

$$Q_j = Q(\nu_j) = \sum_{k=1}^{N_{\rm F}} \cos(2\psi_{jk}) \tag{27}$$

$$U_j = U(\nu_j) = \sum_{k=1}^{N_{\rm F}} \sin(2\psi_{jk}) \tag{28}$$

where

$$\psi_{jk} = (\psi_{\rm in})_j + RM_k \left(\frac{c}{\nu_j}\right)^2. \tag{29}$$

The Fourier transform of eq. (8) is replaced by a discrete Fourier transform to the time-lag domain, with real and imaginary components

$$\mathcal{R}(t_n) = \frac{1}{N_{\rm chan}} \sum_{j=1}^{N_{\rm chan}} \left[Q_j \cos(2\pi t_n \omega_j) + U_j \sin(2\pi t_n \omega_j)\right]$$

$$\mathcal{I}(t_n) = \frac{1}{N_{\rm chan}} \sum_{j=1}^{N_{\rm chan}} \left[U_j \cos(2\pi t_n \omega_j) - Q_j \sin(2\pi t_n \omega_j)\right] \tag{30}$$

evaluated at discrete $t_n = n\delta t - 1/2\delta\nu$, where $\omega_j = (\nu_j - \nu_{\rm c})$.

4.2 Numerical Simulations

The modelling process is conducted as follows.

(i) Artificial Stokes Q and U spectra are generated with the correct λ^2 dependence for a particular set of correlator parameters $(\nu_{\rm c}, \Delta\nu, N_{\rm chan})$ and one or more RM components $(\mathrm{RM}_1 \ldots \mathrm{RM}_{N_{\rm F}})$. These spectra include the (generally small) effects of bandwidth depolarization over the individual channels. This is done by first generating over-sampled spectra and then summing the contributions over each channel to produce the final spectra with the desired number of channels.

(ii) The real and imaginary Fourier transforms are calculated to form the complex valued $\mathcal{P}(t_n)$.

(iii) Peaks in $|\mathcal{P}(t_n)|$ are identified and associated with RM components $\mathrm{RM}_n = (-\pi\nu_{\rm c}t_n)/(2\lambda_{\rm c}^2)$.

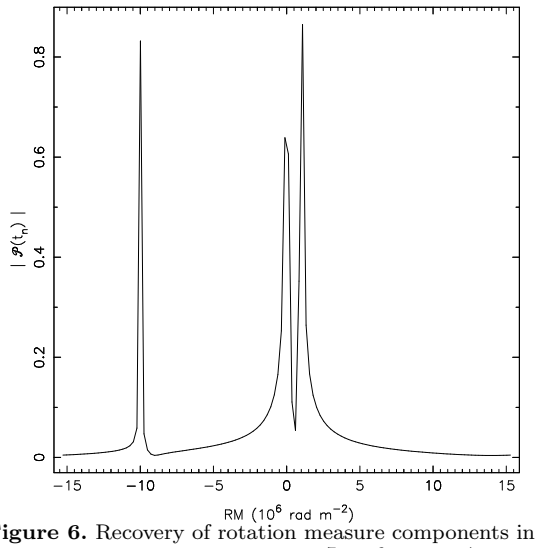

Figure 6. Recovery of rotation measure components in time-lag space. Input RM values were -10^7, 10^6 and 10^4 rad m^{-2}, and the correlator configuration was ($\nu_c = 4.8$ GHz, $\Delta\nu = 8$ MHz, $N_{\rm chan} = 128$).

Note that the central lag channel† contains all signals with $|\mathrm{RM}| < \Delta\mathrm{RM}_{\rm samp}$.

An example of the Fourier transform technique is shown in Fig. 6, where the amplitude spectrum (for a point source) is plotted against the time-lag domain (converted for convenience to RM values at each lag, t_n). The correlator configuration was ($\nu_c = 4.8$ GHz, $\Delta\nu = 8$ MHz, $N_{\rm chan} = 128$) with $\Delta\mathrm{RM}_{\rm samp} = 2.7\times10^5$ rad m^{-2} and $\mathrm{RM}_{\rm max} = 1.7\times10^7$ rad m^{-2}.

The input values of RM $= -10^7$ and 10^6 rad m^{-2} are recovered within $\Delta\mathrm{RM}_{\rm samp}$ as -9.99×10^6 and 1.08×10^6 rad m^{-2} respectively. The third component, RM $= 10^4$ rad m^{-2} which is below $\Delta\mathrm{RM}_{\rm samp}$ falls in one of the two central channels (since $N_{\rm chan}$ is even).

Each of the three components has the approximate delta function appearance (convolved with the bandpass sinc function) expected from eq. (12), but with an asymmetric broadening because of the true λ^2 dependence of the Stokes vectors.

4.3 Noise

In practice, the Q and U spectra will be subject to Gaussian distributed noise. We extend the definition of the Stokes vectors in eq. (27) and eq. (28) to include this term (given with standard deviation σ_ν):

$$Q_{n,\rm obs} = \frac{Q_n + \epsilon_{\rm Q}(\nu_n)}{\sigma_\nu} \tag{31}$$

and similarly for $U_{n,\rm obs}$. Unless otherwise stated, it is assumed that the amplitude of all noise signals is the same for both Stokes Q and U.

The most obvious effect of $\epsilon(\nu_n)$ is to introduce spurious RM signals. Fig. 7 shows the result of adding Gaussian noise with $\sigma_\nu = 2.5$ and $\sigma_\nu = 0.5$ to Q and U for the same correlator configuration and RMs of Fig. 6.

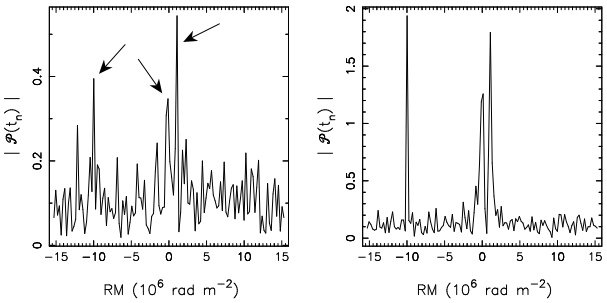

Figure 7. Recovery of rotation measure components in time-lag space with Gaussian distributed noise: (left) $\sigma_\nu = 2.5$; the arrows indicate the real peaks (right) $\sigma_\nu = 0.5$. Input RM values were -10^7, 10^6 and 10^4 rad m^{-2}, and the correlator configuration was ($\nu_c = 4.8$ GHz, $\Delta\nu = 8$ MHz, $N_{\rm chan} = 128$).

As discussed in Section 2.4, the Fourier transform technique optimally recovers RM signals in the low signal-to-noise regime. Here, even for $\sigma_\nu = 2.5$, we can still see the signature delta function peaks of the RM components, but the Gaussian noise has introduced at least one potentially erroneous RM in this example. In general, we find that for a signal-to-noise per channel $(\mathcal{S}/\mathcal{N}_{\rm c}) \gtrsim 1$, the recovery of RM components is not affected by a Gaussian noise component.

Frequency-dependent noise may also occur, as the bandpass determination may become more noisy at the edge or the band or, equivalently, there will be less signal. Whilst this is really a calibration effect (see next section), it is more useful to discuss it here. We can model this as a simple parabola across the bandwidth

$$\epsilon(\nu_n) = \frac{4(\sigma_{\rm max} - \sigma_{\rm min})}{(\Delta\nu)^2}(\nu_n - \nu_{\rm c})^2 + \sigma_{\rm min} \tag{32}$$

where $\sigma_{\rm min}$ is the minimum noise level (assumed to occur in the central frequency channel) and $\sigma_{\rm max}$ is the maximum noise level which occurs in the first and last channel. We find that the amplitude spectrum for a frequency-dependent noise profile is qualitatively equivalent to the 'constant' Gaussian noise case with $\sigma_\nu = \sigma_{\rm max}$.

In summary, Gaussian distributed noise can produce spurious RM signals, but only when $\mathcal{S}/\mathcal{N}_{\rm c} \lesssim 1$.

Let us now examine what the traditional approach would have done with the above example. In Fig. 8, we show the variation in the position angle, ψ, for the same three input RMs ($-10^7, 10^6$ and 10^4 rad m^{-2}) as in Fig. 6 with no noise. The correlator configuration was $\nu_{\rm c} = 1.5$ GHz, $\Delta\nu = 128$ MHz and $N_{\rm chan} = 128$. It is obvious that the ambiguities produced by these very high RMs, and the discontinuities in ψ, would make it impossible to recver the input RMs with a traditional least-squares fit ψ–λ^2.

4.4 Calibration Errors

The spectra will also be subject to various calibration errors. It is important to be able to recognize calibration errors that masquerade as RM signals.

Consider a point source at the phase centre and a single frequency observation. With a perfect calibration, after conversion from the linear or circular correlations, the I,

† if $N_{\rm chan}$ is odd, otherwise central two channels

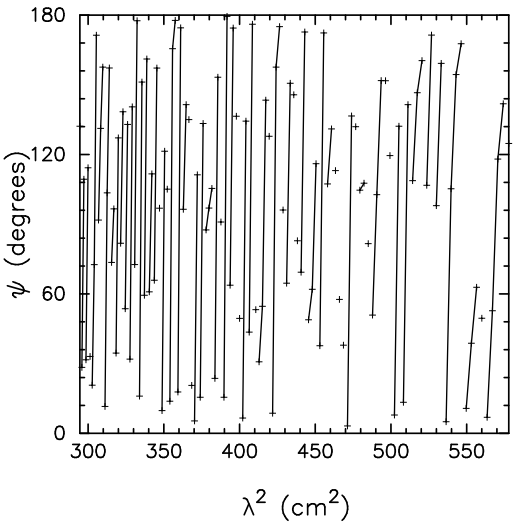

Figure 8. Variation of position angle, ψ, with λ^2 for input RMs $-10^7, 10^6$ and 10^4 rad m^{-2}. The correlator configuration was (ν_c = 1.5 GHz, $\Delta\nu$ = 128 MHz, $N_{\rm chan}$ = 128). A traditional least-squares fit to any subset of λ^2 values would not be able to recover any of the RM components.

Q, U and V visibilities should have phase zero (i.e. be real valued apart from noise). Any gain and leakage calibration errors act to add a complex term to these visibilities. Therefore, if you imaged the mis-calibrated visibilities, the point source would become non-point-like – the flux would be redistributed in some way. Note that the images are real valued (we are imaging the sky); the complex errors in the visibilities affect the **real spatial** structure of the source, they do not make it imaginary.

Now consider a multichannel observation of our point source. If we made (naturally weighted) multichannel Q and U images from this observation, we could extract (real-valued) Q and U spectra at the location of the point source. Alternatively, we could average the real part of the Q and U visibilities; this would make the same spectra.

If we ignore the fact that the **shape** of the source has been changed by the calibration errors, we need concern ourselves only with the effect on the real part of the visibilities that the calibration errors have. We are also mainly interested in frequency-dependent errors, as these will affect the character of the RM spectrum.

Calibration and instrumental errors can include: a DC offset across the bandpass, DC; a frequency-dependent gain, $F(\nu_j)$ (assumed sinusoidal across $\Delta\nu$); and a polarization leakage calibration error term, $D(\nu)$ (modelled as a linear ramp with gradient $m_{\rm leak}$ across $\Delta\nu$). This is not an exhaustive list of all the possible instrumental and calibration terms (or their functional form) which may affect the detection of RMs, but gives an indication of how strong such terms would have to be to produce spurious RM signals.

Note also that first-order gain and leakage errors manifest themselves as fractions of total intensity added to Q and U. This is why they are included here as additive errors. Including these errors, the definitions of the Stokes vectors are:

$$Q_{n,\rm obs} = \frac{Q_n + DC_{\rm Q} + F_{\rm Q}(\nu_n) + D_{\rm Q}(\nu_n) + \epsilon_{\rm Q}(\nu_n)}{\sigma_\nu} \qquad (33)$$

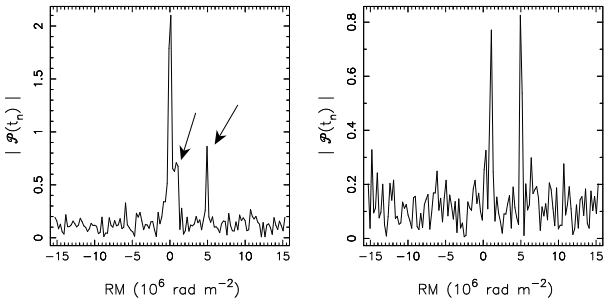

Figure 9. Effect of a DC offset in Stokes Q and U on the recovery of rotation measures. Input RM values are 10^6 and 5×10^6 rad m^{-2} (indicated by arrows). Correlator configuration was (ν_c = 4.8 GHz, $\Delta\nu$ = 8 MHz, $N_{\rm chan}$ = 128). Noise components: Gaussian noise $\sigma_\nu = 1$ and (left) $DC_{\rm Q} = 3$, $DC_{\rm U} = 0$; the arrows indicate the real peaks (right) $DC_{\rm Q} = 0.1$, $DC_{\rm U} = -0.2$.

and similarly for $U_{n,\rm obs}$.

A DC offset in Q and U may arise from the correlator. Generally these are different from baseline to baseline; in the simplest case where all baselines have the same offset, the error is indistinguishable from a point source at the phase centre. This will appear in lag space as a signal with RM $< \Delta{\rm RM}_{\rm samp}$, as it is a component which does not vary across the bandwidth. If the DC offset is greater than $\sigma_\nu > 1$, then the amplitudes of all other RM signals are reduced and may become comparable to the noise signal. In practice, any DC offset in Q and U should be small, and so this error should not affect the detection of RM components. This is demonstrated in Fig. 9 where we have two RM components, a noise term, and a DC signal. In the left-hand panel, there is a strong signal in the central lag channel caused by the offsets $DC_{\rm Q} = 3$ and $DC_{\rm U} = 0$, but the two RM components (RM = 10^4 and 2×10^5 rad m^{-2}) are still detectable. This DC signal disappears within the noise if the DC offsets are reduced, as can be seen in the right-hand panel.

Next we consider the effect of a frequency-dependent gain error, $F(\nu_n)$, which is modelled as a weakly varying sinusoidal component in Q and U. The character of an actual frequency-dependent error is observation dependent, and so our choice of a sinusoid is somewhat arbitrary. We have:

$$F(\nu_n) = \mathcal{A}_F \sin\left(\frac{2\pi N_{\rm cycle} n}{N_{\rm chan}} + \phi_{\rm Q,U}\right) \qquad (34)$$

with $N_{\rm cycle}$ cycles across the bandwidth, where n is the frequency channel number, $\mathcal{A}_F$ the signal amplitude and $\phi_{Q,U}$ allows for a phase difference in the gain error between Q and U.

In the amplitude spectrum, this signal would appear as a pair of peaks at $t = \pm N_{\rm cycle}/\Delta\nu$, corresponding to RM = $\pm N_{\rm cycle}{\rm RM}_{\rm min}$, as shown in Fig. 10. For this fault signal to be detected requires $N_{\rm cycle} > 1$, otherwise it will fall in the central time-lag channel(s). The strength of the signal in lag space depends on the amplitude of the gain error, $\mathcal{A}_F$. The addition of the phase term $\phi_{\rm Q,U}$ changes the relative heights of the two delta functions in time-lag space.

For $\mathcal{S}/\mathcal{N}_{\rm c} < 1$, we find that a sinusoidal frequency-dependent gain error could result in a false RM detection if $\mathcal{A}_F \gtrsim 0.4$. Unless the calibration is poor, the amplitude of any frequency-dependent gain should be small, and hence will be lost within the noise signal in time-lag space.

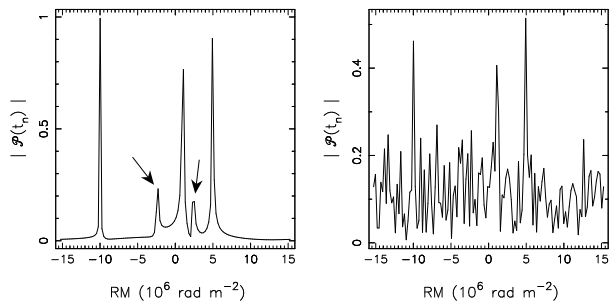

Figure 10. Effect of a frequency-dependent gain error on the recovery of rotation measures. Input RM values were -10^7, 10^6 and 5×10^6 rad m^{-2}. The correlator configuration was (ν_c = 4.8 GHz, $\Delta\nu$ = 8 MHz, $N_{\rm chan}$ = 128). Both panels have a gain error with $\mathcal{A}_F = 0.4$, $N_{\rm cycle} = 10$. (left) With no Gaussian noise, fault signals are detected at RM = $\pm\, 2.2 \times 10^6$ rad m^{-2}, as indicated by the arrows. (right) On the addition of Gaussian noise with $\sigma_\nu = 2$, the fault signals are comparable to the amplitude noise level.

A polarization observation must be calibrated to allow for the fact that the feeds are not perfect. That is, the polarization ellipse of linearly polarized feeds will be slightly elliptical, and for circularly polarized feeds, slightly non-circular. These are characterized by 'leakage' terms, and they describe the amount of fully polarized signal that is detected by the orthogonal polarization (e.g. how much completely polarized signal in the X direction is detected by the Y feed). There is generally a frequency dependence in the leakages, although its exact form is design dependent. Often this frequency dependence is not calibrated.

We model any uncalibrated leakage dependence as a simple gradient across the bandwidth. Since the gradient will be either a monotonically increasing or decreasing function across the bandwidth, the Fourier transform of this component will be a signal in the central time lag channel(s) (i.e. below the RM sampling resolution). The amplitude of this fault signal depends on the gradient of the leakage – a larger gradient gives a greater amplitude in lag space. If there is also Gaussian noise present, a gradient $m_{\rm leak} > \sigma_\nu$ produces a large signal in the zero-lag channel, but the RM components are still detectable. A large gradient should be obvious by examining Q and U, whereas a weak gradient across $\Delta\nu$ slightly reduces the amplitudes of the RM components in $|\mathcal{P}(t_n)|$.

The exact form of a non-calibrated, frequency-dependent leakage error depends very much on the design of the hardware. For example, there may well be small-scale variations (trapped modes) over a few channels, or larger quasi-sinusoidal variation. The latter would show up as a spurious RM signal (see above). The important thing is to calibrate it out as much as possible, and be aware of the residual error form.

We have now shown qualitatively that a range of possible calibration errors does not adversely affect the recovery of RM signals with the Fourier transform method, even when the $\mathcal{S}/\mathcal{N}_c$ is small. Caution must be used when identifying RM components in the central lag channel(s) – any RM which is below $\rm RM_{samp}$ will occur here, but may be mixed in with fault signals caused by the DC offset or leakage gradients from the calibration.

5 SUMMARY

The traditional approach to measuring RM values from radio polarimetric data consists of fitting linear polarization position angles obtained at different wavelengths to a λ^2 law. This method yields a singly valued RM distribution, and is hindered by the $n * \pi$ ambiguity, bandwidth depolarization, and bad characteristics at low signal-to-noise ratios. Additionally, it will generate incorrect results if the RM distribution is not singly valued.

We have described a new technique where the RM distribution is recovered directly from the Fourier transform of the frequency spectrum. This approach has the following features.

- It has wide astrophysical applicability and is important for any object with polarized emission that has traversed regions of high electron density or magnetic field. Such regions are galactic nuclei, the broad line regions of AGNs and radio galaxies.
- It is sensitive to RM signals over a finite range. The maximum detectable RM is

$$RM_{\rm max} = \frac{\pi\nu_c}{4\lambda_c^2\delta\nu}. \tag{35}$$

Any signal less than the RM sampling criterion,

$$\Delta RM_{\rm samp} = \frac{\pi\nu_c}{2\lambda_c^2\Delta\nu}, \tag{36}$$

will fall into the central bin of the RM spectrum (the Fourier transform of the frequency spectrum).
By choosing the appropriate correlator configuration, a wide range of RMs can be measured (see Appendix A).

- There is no $n * \pi$ ambiguity problem.
- Noise is correctly handled, allowing the detection of weaker signals than with the traditional method.
- Provided unresolved spatial RM gradients do not *totally* depolarize the signal in each channel, the spatially unresolved RM distribution can be recovered. We can also recover the weighted polarization state incident upon each component in the RM distribution.
- Because it depends upon the use of closely spaced frequencies, while handling noise correctly, this technique can, in principle, provide access to very large RMs. The range depends upon the exact frequency configurations the correlator of a particular telescope provides. A Table relevant to the Australia Telescope Compact Array is shown in Appendix A. Its upper limit is $\sim 10^9$ rad m $^{-2}$.
- Polarization spectral index effects are negligible.
- Difficulties with bandwidth depolarization are alleviated (but not defeated) since the technique is based on observations with many closely spaced channels. If the RM is sufficiently large that a single channel is fully bandwidth depolarized, then our method cannot help.

One might also consider using this method with data consisting of several blocks of channels in different bands. However, in this case, the RM response function would have high side lobes because of the poor frequency sampling (see also de Bruyn (1996)); deconvolution could be considered. All assumptions based on narrow fractional bandwidth would also need scrutiny if one pursued this path.

We suggest that the procedure for applying this technique to multichannel full polarization synthesis data is:

(i) calibrate the data, taking care to make frequency dependent calibrations for gains (the bandpass) and polarization leakage;

(ii) make multichannel images (called cubes – RA-DEC-Freq) for Stokes Q and U (of course V is always good for instrumental error checks);

(iii) if there is a strong signal in the zero lag which is not of interest, you might subtract the average of Q and U (i.e. for each spatial pixel, find the average of the spectrum and subtract it) from the cubes. This forces the zero lag to be identically zero which means it will not ring through the lag cube (which might otherwise mask weak, large-value RMs). The ringing occurs because the frequency spectrum has sharp cutoffs;

(iv) do a complex Fourier transform of the frequency axis (usually the third) of the image $Q + iU$ to the time domain, creating a complex RA-DEC-Time image. The value of this image is $\mathcal{P}(t)$;

(v) create the amplitude image from $\mathcal{P}(t)$ and search for RM peaks. The time axis can be converted to RM with eq. (11).

ACKNOWLEDGMENTS

We thank Bob Sault and Agris Kalnajs for their interest in this work. In particular, Bob had the insight that there was no RM aliasing problem.

APPENDIX A: AUSTRALIA TELESCOPE COMPACT ARRAY RM OBSERVATIONAL PARAMETERS

Whilst we have written this paper in largely general terms, we provide here a table (Table A1) relevant to the Australia Telescope Compact Array, indicating the range of rotation measures accessible to this instrument. The ATCA correlator always provides multiple channels – there is no traditional broadband mode of observation with this instrument.

Table A1. Rotation measure ranges accessible to the Australia Telescope Compact Array. This is not an exhaustive list of all possible configurations. The RM resolution of each set-up is $\Delta\mathrm{RM}_{\mathrm{samp}} = \mathrm{RM}_{\mathrm{min}}$.

ν (GHz)	λ (cm)	$\Delta\nu$ (MHz)	N_{chan}	$\mathrm{RM}_{\mathrm{min}}$ (rad m^{-2})	RM_{max} (rad m^{-2})
1.4	22	128	32	350	5500
		64	64	690	2.2×10^4
		16	256	2800	3.5×10^5
		8	512	5500	1.4×10^6
		4	1024	1.1×10^4	5.7×10^6
2.3	13	128	32	1700	2.7×10^4
		64	64	3300	1.1×10^5
		16	256	1.3×10^4	1.7×10^6
		8	512	2.7×10^4	6.9×10^6
		4	1024	5.4×10^4	2.7×10^7
5.0	6	128	32	1.7×10^4	2.7×10^5
		64	64	3.4×10^4	1.1×10^6
		16	256	1.4×10^5	1.7×10^7
		8	512	2.7×10^5	7.0×10^7
		4	1024	5.5×10^5	2.8×10^8
10.0	3	128	32	1.4×10^5	2.2×10^6
		64	64	2.7×10^5	8.7×10^6
		16	256	1.1×10^6	1.4×10^8
		8	512	2.2×10^6	5.6×10^8
		4	1024	4.4×10^6	2.2×10^9

Address for Correspondence

N.E.B. Killeen
Australia Telescope National Facility
P.O. Box 76
Epping
NSW 1710 Australia

Email: nkilleen@atnf.csiro.au
Fax: +61–2–9372–4400
Phone: +61–2–9372–4261

REFERENCES

Conway R.G., Kronberg P.P., MNRAS, 1969, 142, 11
D'Addario L.R., 1989, Chapter 4 in "Synthesis Imaging in Radio Astronomy", Astronomical Society of the Pacific Conference Series, Volume 6
de Bruyn A.G., 1996, NFRA Internal note 655, March 1996
Faraday M., 1844, Experimental researches in electricity. London: R Taylor 1844. Repr. New York: Dover 1952
Kraus J.D., 1966, "Radio Astronomy", McGraw-Hill, New York
Stokes G.G., 1852, Trans. Camb. Phil. Soc. 9, 399
Thomson A.R., Moran J.M. and Swenson G.W., 1994, Interferometry and Synthesis in Radio Astronomy, Krieger Publishing Company, Florida
Vinokur M., 1965, Ann. d'Ap., 28, 412
Wardle J.F.L., Kronberg P.P, 1974, Ap.J., 194, 249